J Eng Math (2008) 62:51–65
DOI 10.1007/s10665-007-9156-4

Suppression of vibration localization in non-axisymmetric periodic structures

Shahram M. Shahruz

Received: 1 December 2006 / Accepted: 14 May 2007 / Published online: 7 July 2007

Abstract In this paper, mistuned non-axisymmetric periodic structures are considered. In such a structure, vibration localization, which results in large vibrations in some components of the structure, can occur. Such a behavior is due to mistunings in the structure components, small damping, and weak coupling between components. The efficacy of a passive technique (previously proposed by the author for axisymmetric structures) in suppressing vibration localization in mistuned non-axisymmetric periodic structures is examined. The technique is based on adding small components between components of structures. It is first shown numerically that the added components suppress vibration localization in mistuned structures. Then, this conclusion is rigorously proved by using the singular perturbation method. Application of the technique studied in the paper to comb drives of micro electro-mechanical systems (MEMS) is given.

Keywords Comb drives of micro electro-mechanical systems (MEMS) · Mistuned non-axisymmetric periodic structures · Mistunings · Singular perturbation method · Vibration localization

1 Introduction

In this paper, suppression of vibration localization in periodic structures is studied. The work presented here is a continuation of what has been reported in [1–3]. This paper is different from [1–3] in two respects: (i) periodic structures considered in [1–3] are axisymmetric, where each component of a structure is surrounded by two components. The periodic structures considered in this paper, however, have two components at their ends that have only one neighboring component; (ii) components of structures are modeled by an approach different from that in [1–3].

Vibration localization can occur in periodic structures. This phenomenon has been studied by numerous researchers; see, e.g., [1–13] and references therein. A brief description of vibration localization is as follows. Components of periodic structures are designed to have identical geometry (dimensions) and material properties. In reality, however, components of fabricated structures are not exactly identical and differ slightly from each other. In this case, the structure is said to be *mistuned*. The differences between components of a mistuned structure and a desired

S. M. Shahruz (✉)
Berkeley Engineering Research Institute, P. O. Box 9984, Berkeley, CA 94709, USA
e-mail: shahruz@cal.berkeley.edu

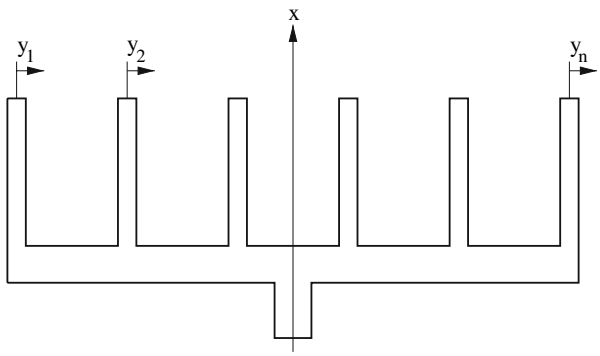

Fig. 1 A non-axisymmetric periodic structure, such as a comb drive used in MEMS. Components at both ends of the structure have only one neighboring component. The structure components can vibrate in the directions of $y_1, y_2, \ldots, y_n$. In an axisymmetric structure each component of the structure is surrounded by two components

component are called *mistunings*. Mistunings are typically due to slight differences in the geometry and material properties of components which are mainly introduced during fabrication.

If there were no mistunings in components of a periodic structure, then the dynamics of components would have been (almost) the same. Small mistunings, however, can cause significant differences in the dynamics of components. For instance, consider a mistuned structure whose components are subjected to the same harmonic input. In such a structure, near the structure fundamental frequency, some components may vibrate with small amplitudes, while some others may vibrate with significantly larger amplitudes. This behavior is known as *vibration localization*. Roughly speaking, vibration localization in a periodic structure is due to mistunings in the structure components, small damping, and weak coupling between components.

Vibration localization in a periodic structure is mostly considered undesirable since it causes large vibrations and stresses leading to possible damage to some of the structure components. Several researchers have devised means of reducing vibration localization; see, e.g., [1–3,6,8,12]. In [1–3], a novel passive technique is proposed by which vibration localization in mistuned axisymmetric periodic structures is suppressed.

Suppression of vibration localization in non-axisymmetric periodic structures is an important problem awaiting viable solutions. An example of such a structure is a comb drive.

Comb drives are miniaturized comb-like structures used in many micro-electro-mechanical systems (MEMS). For instance, they are used in actuators of micro grippers, X–Y micro stages, micro-mechanical gear trains, vibromotors, data-storage devices, and optical switches; or they are used in sensors such as force-balanced accelerometers, laterally oscillating gyroscopes, friction test devices, voltmeters, and scanning probe devices; see, e.g., [14–27] and references therein.

Comb drives consist of two interdigiated comb-like structures. One comb is fixed and the other one is attached to a compliant structure, and hence is movable. When a voltage difference is applied between the combs, an electrostatic driving force is generated that moves the movable comb towards the fixed one. To generate a reasonably large driving force, combs should have many fingers, because the generated force is linearly proportional to the number of fingers. A typical comb is shown in Fig. 1. Fingers of most comb drives are designed to have identical geometry and material properties. That is, comb drives are designed to be periodic structures.

The position of the movable comb is controlled by the generated electrostatic force and the mechanical restoring force of the compliant structure to which it is attached. The driving force moves the movable comb axially in the x-direction; see Fig. 1. Forces applied to a finger of the movable comb by the two adjacent fingers of the fixed comb are balanced. However, any perturbation in these forces would result in an offset force that pulls the finger sideways, transversal to the x-direction. This behavior is known as electro-mechanical side instability (also known as side snap-over); see, e.g., [21,23] and references therein. The sideway motion of fingers, which can be intensified by vibration localization, severely limits the large stable travel range of the movable comb. Such motion can result in the adhesion of the movable fingers to the fixed ones, and hence damage the comb drive; see, e.g., [16, p. 133]. Therefore, it is important to design comb drives, the fingers of which move sideways as little as possible.

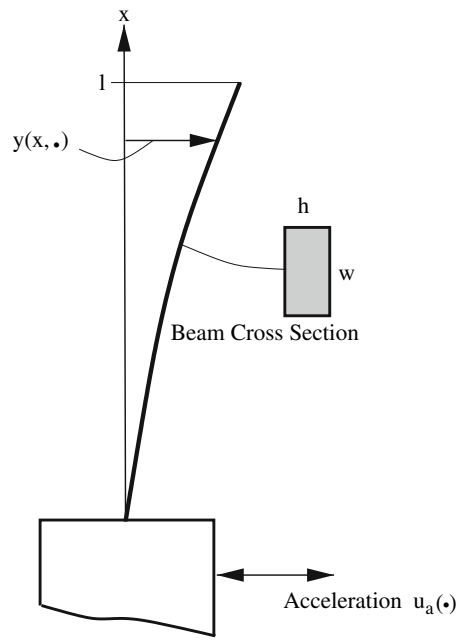

Fig. 2 A schematic of a cantilever beam. The beam is mounted on a base to which the acceleration $u_a(\cdot)$ is applied

In this paper, it is shown that vibration localization in mistuned non-axisymmetric periodic structures can be suppressed by the technique proposed in [1–3]. The organization of the paper is as follows. In Sect. 2, a mathematical model of mistuned non-axisymmetric periodic structures is presented. In Sect. 3, it is explained how to determine the possibility of the occurrence of vibration localization in such structures. In Sect. 4, the passive technique of suppressing vibration localization proposed in [1–3] is adopted. This technique is based on adding small components between the structure components. Via an example of a comb drive, it is illustrated that the added components suppress vibration localization in mistuned non-axisymmetric periodic structures. In Sect. 5, it is rigorously proved that the added components suppress vibration localization. The proof is established by using a dichotomy in the dynamics of the structure to which the small components are added, and by applying the singular perturbation method.

2 A model of mistuned non-axisymmetric periodic structures

In this section, a mathematical model of a vibrating cantilever beam is first presented. Then, based on the beam model, a mathematical model of mistuned non-axisymmetric periodic structures with n components, such as that shown in Fig. 1, is derived. It is remarked that the approach to the modeling of periodic structures in this paper differs from that in [1–3]. In this paper, the structure components are considered as (elastic) cantilever beams, whereas in [1–3], the structure components are considered as rigid beams connected to a rigid base by torsional springs.

2.1 A mathematical model of a vibrating cantilever beam

In Fig. 2, a schematic of a cantilever beam is shown. The length, width, and thickness of the beam are denoted by l, w, and h, respectively. The mass density and the modulus of elasticity of the beam are denoted by ρ and E, respectively. The beam is mounted on a base to which an acceleration $u_a(\cdot)$ is applied. Due to this external input, the beam vibrates transversally. The transversal displacement of the beam at an $x \in [0, l]$ and a $t \geq 0$ is denoted by $y(x, t) \in \mathbb{R}$.

With this set-up, a mathematical model describing the dynamics of the beam has been derived in [28–30]. This model, which is partially adopted in this paper, is described briefly in the following.

The transversal displacement of the beam is written as

$$y(x,t) = \phi(x)q(t), \tag{1}$$

for all $x \in [0, l]$ and $t \geq 0$. In Eq. 1, the real- and scalar-valued function $x \mapsto \phi(x)$, known as the trial or shape function, is

$$\phi(x) = a\left(\frac{x}{l}\right)^2 - b\left(\frac{x}{l}\right)^3, \tag{2}$$

for all $x \in [0, l]$, where

$$a = 4.7896, \quad b = 2.1976. \tag{3}$$

The real- and scalar-valued function $t \mapsto q(t)$ in Eq. 1, which is known as the generalized coordinate, is the solution of the following second-order ordinary differential equation:

$$m\,\ddot{q}(t) + k\,q(t) = -f\,u_a(t), \quad q(0) = 0, \quad \dot{q}(0) = 0, \tag{4}$$

for all $t \geq 0$, where

$$m = a_1\rho whl, \quad k = \frac{a_2 E w h^3}{3l^3}, \quad f = a_3\rho whl, \tag{5}$$

with

$$a_1 = \frac{a^2}{5} - \frac{2ab}{6} + \frac{b^2}{7} = 1.7694, \tag{6a}$$

$$a_2 = a^2 - 3ab + 3b^2 = 5.8517, \tag{6b}$$

$$a_3 = \frac{a}{3} - \frac{b}{4} = 1.0471. \tag{6c}$$

The unique solution of system (4) for $t \mapsto q(t)$ can be obtained. When this solution is substituted in Eq. 1, the transversal displacement of the undamped beam is (approximately) obtained.

It can be easily verified that $x \mapsto \phi(x)$ in Eq. 2 is a monotonically increasing function over the interval $[0, 2al/(3b)] = [0, 1.453l]$. Thus, $x \mapsto \phi(x)$ is maximum at $x = l$. Therefore, the absolute value of the displacement of the tip of the beam, $|y(l, t)|$, is the largest for all $t \geq 0$.

2.2 A mathematical model of mistuned periodic structures

In Fig. 1, a periodic structure with n components is shown. Each component is considered as a cantilever beam. The length, width, and thickness of the ith beam for an $i = 1, 2, \ldots, n$ are denoted by l_i, w_i, and h_i, respectively. The transversal displacement of the ith beam is written as

$$y_i(x,t) = \phi(x)\,q_i(t), \tag{7}$$

for all $x \in [0, l_i]$ and $t \geq 0$, where $x \mapsto \phi(x)$ is that in Eq. 2 and $t \mapsto q_i(t)$ is the generalized coordinate of the beam.

Using the model for one cantilever beam in Eq. 4, a mathematical model of the structure can be obtained as

$$M\ddot{\mathbf{q}}(t) + \alpha M\dot{\mathbf{q}}(t) + K\mathbf{q}(t) = -\mathbf{f}\,u_a(t), \tag{8}$$

for all $t \geq 0$. In Eq. 8, the vector of generalized coordinates is

$$\mathbf{q}(t) = [q_1(t) \quad q_2(t) \ldots q_n(t)]^T \in \mathbb{R}^n, \tag{9}$$

for all $t \geq 0$. The initial conditions of system (8) are $\mathbf{q}(0) = \mathbf{0}_n$ and $\dot{\mathbf{q}}(0) = \mathbf{0}_n$, where $\mathbf{0}_n$ denotes the zero vector in $\mathbb{R}^n$. The input (influence) vector through which the acceleration $u_a(\cdot)$ is applied to system (8) is

$$\mathbf{f} = [f_1 \quad f_2 \ \ldots \ f_n]^T \in \mathbb{R}^n, \tag{10}$$

where f_i is computed via Eq. 5 for all $i = 1, 2, \ldots, n$. The mass and stiffness matrices of system (8) are, respectively,

$$M = \text{diag}[m_1, m_2, \ldots, m_n] \in \mathbb{R}^{n\times n}, \tag{11a}$$

$$K = \begin{bmatrix} k_1 + k_c & -k_c & 0 & 0 & \cdots & 0 & 0 & 0 \\ -k_c & k_2 + 2k_c & -k_c & 0 & \cdots & 0 & 0 & 0 \\ 0 & -k_c & k_3 + 2k_c & -k_c & \cdots & 0 & 0 & 0 \\ \vdots & \vdots & \vdots & \vdots & \cdots & \vdots & \vdots & \vdots \\ 0 & 0 & 0 & 0 & \vdots & -k_c & k_{n-1} + 2k_c & -k_c \\ 0 & 0 & 0 & 0 & \cdots & 0 & -k_c & k_n + k_c \end{bmatrix} \in \mathbb{R}^{n\times n}, \tag{11b}$$

where m_i and k_i are computed via Eq. 5 for all $i = 1, 2, \ldots, n$, and the positive real number k_c represents the coupling between two adjacent beams. The damping proportionality factor in system (8) is denoted by the positive real number α.

Two remarks regarding system (8) are in order: (i) the adjacent components of the structure are coupled. It is difficult to model and quantify the coupling of components. In this paper, it is assumed that the structure components are coupled via massless springs of stiffness k_c; (ii) the structure components are designed to have their dimensions l_i, w_i, and h_i equal to desired values l_d, w_d, and h_d, respectively, for all $i = 1, 2, \ldots, n$. In reality, however, the dimensions of the fabricated components are different from the desired values. That is, there are mistunings in the structure.

To study the dynamics of the mistuned structure, the following state-space representation of system (8) will be used:

$$\frac{\mathrm{d}}{\mathrm{d}t}\begin{bmatrix} \mathbf{q}(t) \\ \dot{\mathbf{q}}(t) \end{bmatrix} = A\begin{bmatrix} \mathbf{q}(t) \\ \dot{\mathbf{q}}(t) \end{bmatrix} + b_f u_a(t), \quad \begin{bmatrix} \mathbf{q}(0) \\ \dot{\mathbf{q}}(0) \end{bmatrix} = \begin{bmatrix} \mathbf{0}_n \\ \mathbf{0}_n \end{bmatrix}, \tag{12a}$$

$$\begin{bmatrix} y_1(l_1, t) \\ y_2(l_2, t) \\ \vdots \\ y_n(l_n, t) \end{bmatrix} = C\begin{bmatrix} \mathbf{q}(t) \\ \dot{\mathbf{q}}(t) \end{bmatrix}, \tag{12b}$$

for all $t \geq 0$, where $y_i(l_i, t) = \phi(l_i)q_i(t)$ denotes the displacement of the tip of the ith beam for an $i = 1, 2, \ldots, n$, and

$$A = \begin{bmatrix} 0 & I_n \\ -M^{-1}K & -\alpha I_n \end{bmatrix} \in \mathbb{R}^{2n\times 2n}, \quad b_f = \begin{bmatrix} \mathbf{0}_n \\ -M^{-1}\mathbf{f} \end{bmatrix} \in \mathbb{R}^{2n}, \tag{13a}$$

$$C = [a_4 I_n \quad 0] \in \mathbb{R}^{n\times 2n}, \tag{13b}$$

with

$$a_4 = a - b = 2.5920, \tag{14}$$

and I_n denotes the $n \times n$ identity matrix.

Vibration localization in system (8) is studied via the representation in Eq. 12.

3 Analysis based on transfer functions

In studying vibration localization in mistuned periodic structures, transfer functions from the applied input to structure displacements play an important role; see [1–3]. Let the transfer function from the applied acceleration to the displacement of the tip of the ith beam for an $i = 1, 2, \ldots, n$ be denoted by $g_i(s)$. From Eqs. 12 and 8, it follows that

$$\begin{bmatrix} g_1(s) \\ g_2(s) \\ \vdots \\ g_n(s) \end{bmatrix} = C(sI_{2n} - A)^{-1} b_f = -a_4(Ms^2 + \alpha Ms + K)^{-1}\mathbf{f}, \tag{15}$$

where A, b_f, and C are given by Eq. 13. To each transfer function $g_i(s)$ there corresponds an H_∞-norm defined by

$$\|g_i\|_\infty := \max_{\omega \in \mathbb{R}} |g_i(\mathrm{j}\omega)|, \tag{16}$$

where $\mathrm{j} = \sqrt{-1}$. The norm $\|g_i\|_\infty$ corresponds to the global maximum of the Bode magnitude plot of $g_i(s)$. By use of the state-space representation in Eq. 12, the transfer functions in Eq. 15 and their corresponding H_∞-norms can be conveniently computed by MATLAB programs; see [31].

The occurrence of vibration localization due to mistunings is easily determined when $\|g_1\|_\infty, \|g_2\|_\infty, \ldots, \|g_n\|_\infty$ are known. If $\|g_i\|_\infty$ for at least one $i = 1, 2, \ldots, n$ is much larger than the H_∞-norms of the other transfer functions, then vibration localization occurs. In other words, if $\|g_1\|_\infty, \|g_2\|_\infty, \ldots, \|g_n\|_\infty$ do not differ much from each other, vibration localization does not occur.

To illustrate vibration localization due to mistunings, an example is now given.

Example 3.1 Let the structure in Fig. 1 be a comb drive made of silicon with the following material properties:

$$\rho = 2329\ \mathrm{kg/m^3}, \quad E = 15 \times 10^{10}\ \mathrm{N/m^2}. \tag{17}$$

Let the comb drive have six fingers. The desired dimensions of the fingers are

$$l_d = 100\,\mu\mathrm{m}, \quad w_d = 7\,\mu\mathrm{m}, \quad h_d = 2\,\mu\mathrm{m}. \tag{18}$$

Furthermore, let the coupling stiffness and the damping proportionality factor in system (8) be, respectively,

$$k_c = 1\ \mathrm{N/m}, \quad \alpha = 15{,}000\ \mathrm{s^{-1}}. \tag{19}$$

With this set-up, several studies are conducted:

Study 1) No mistuning: Let there be no mistunings. That is, let the dimensions of the fingers l_i, w_i, and h_i be equal to l_d, w_d, and h_d, respectively, for all $i = 1, 2, \ldots, 6$. The displacements of the tips of the fingers are related to the applied acceleration by transfer functions $g_1(s), g_2(s), \ldots, g_6(s)$ obtained via Eq. 15. The H_∞-norms of these transfer functions are computed using MATLAB; they are

$$\|g_1\|_\infty = \|g_2\|_\infty = \cdots = \|g_6\|_\infty = 0.6068 \times 10^{-10}\ \mathrm{s^2}. \tag{20}$$

Since there is no mistuning, a same value for the H_∞-norms is expected: no mistuning implies no vibration localization.

The Bode magnitude plots of $g_1(s), g_2(s), \ldots, g_6(s)$ are depicted in Fig. 3. It is remarked that the transfer functions corresponding to the fingers at both ends of the comb drive are slightly different from those corresponding to the other fingers since they have only one neighboring finger. Nevertheless, the differences are not discernible and the Bode magnitude plots of transfer functions corresponding to all fingers overlap.

Study 2) Effect of mistunings: Let there be mistunings. For instance, let

$$\begin{array}{lll} l_1 = 104\,\mu\mathrm{m}, & w_1 = 6.7\,\mu\mathrm{m}, & h_1 = 1.9\,\mu\mathrm{m}, \\ l_2 = 102\,\mu\mathrm{m}, & w_2 = 7.05\,\mu\mathrm{m}, & h_2 = 2\,\mu\mathrm{m}, \\ l_3 = 105\,\mu\mathrm{m}, & w_3 = 7.02\,\mu\mathrm{m}, & h_3 = 1.9\,\mu\mathrm{m}, \\ l_4 = 97\,\mu\mathrm{m}, & w_4 = 6.8\,\mu\mathrm{m}, & h_4 = 2.02\,\mu\mathrm{m}, \\ l_5 = 105\,\mu\mathrm{m}, & w_5 = 6.85\,\mu\mathrm{m}, & h_5 = 2\,\mu\mathrm{m}, \\ l_6 = 99\,\mu\mathrm{m}, & w_6 = 7\,\mu\mathrm{m}, & h_6 = 1.99\,\mu\mathrm{m}. \end{array} \tag{21}$$

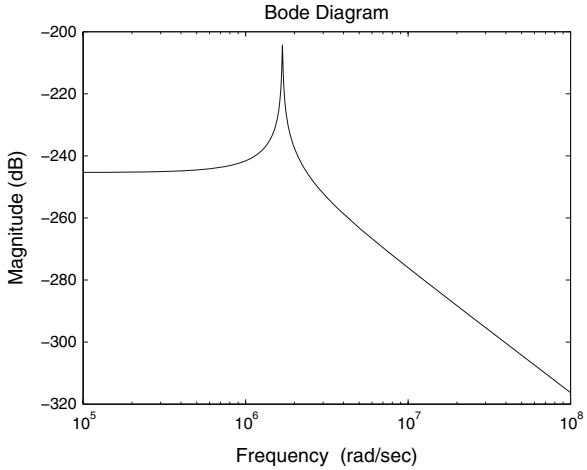

Fig. 3 The Bode magnitude plots of six transfer functions corresponding to six fingers of the comb drive in Example 3.1 when there are no mistunings. The plots overlap

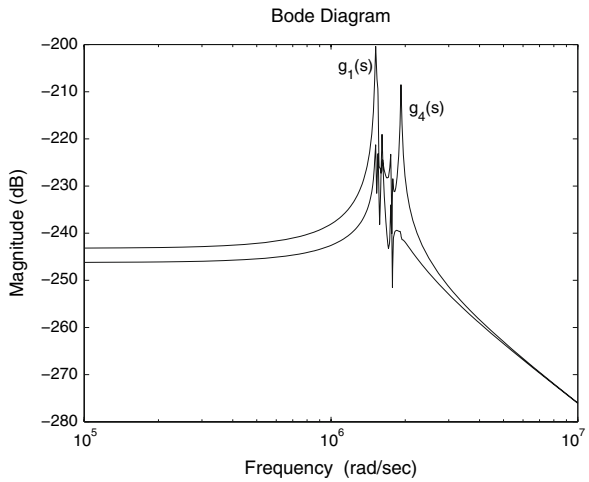

Fig. 4 The Bode magnitude plots of $g_1(s)$ and $g_4(s)$ corresponding to fingers 1 and 4 of the comb drive in Example 3.1 when there are mistunings. Since $\|g_1\|$ is the largest, vibration localization occurs in finger 1

It should be remarked that in reality the lengths, widths, and thicknesses of the fingers are not exactly known; it is only known that they are close to the desired values l_d, w_d, and h_d, respectively.

The H_∞-norms of $g_1(s), g_2(s), \ldots, g_6(s)$ in the presence of mistunings are computed using MATLAB; they are

$$\begin{aligned} &\|g_1\|_\infty = 0.9584 \times 10^{-10}\,\mathrm{s}^2, \quad \|g_2\|_\infty = 0.3827 \times 10^{-10}\,\mathrm{s}^2, \quad \|g_3\|_\infty = 0.5386 \times 10^{-10}\,\mathrm{s}^2, \\ &\|g_4\|_\infty = 0.3750 \times 10^{-10}\,\mathrm{s}^2, \quad \|g_5\|_\infty = 0.7306 \times 10^{-10}\,\mathrm{s}^2, \quad \|g_6\|_\infty = 0.2997 \times 10^{-10}\,\mathrm{s}^2. \end{aligned} \tag{22}$$

It is clear that the H_∞-norms are appreciably different from each other; in particular, $\|g_1\|_\infty$ is larger than the other norms and those in Eq. 20. Thus, vibration localization occurs.

The Bode magnitude plots of $g_1(s)$ and $g_4(s)$ are depicted in Fig. 4. (The Bode magnitude plots of the other transfer functions are not plotted in Fig. 4 since the figure would have been densely cluttered by plots.) These plots are different from each other and from those in Fig. 3. It is also noted that, due to mistunings and coupling, even though small, each finger of the comb drive has several resonant frequencies, unlike the case where there were no mistunings.

4 Suppression of vibration localization

In this section, it is shown that the passive technique in [1–3] suppresses vibration localization in mistuned non-axisymmetric periodic structures. The proposed technique desensitizes $\|g_1\|_\infty, \|g_2\|_\infty, \ldots, \|g_n\|_\infty$ to slight mistunings in components of structures. This technique is based on adding small components between the components of structures.

Let the components of the periodic structure in Fig. 1 be numbered by $1, 2, \ldots, n$. These components are called the *principal components*. These components are supposed to have their dimensions l_i, w_i, and h_i equal to desired values l_d, w_d, and h_d, respectively, for all $i = 1, 2, \ldots, n$.

Let the structure be augmented by adding $n-1$ small components between the principal components as shown in Fig. 5. The added components are numbered by $n+1, n+2, \ldots, 2n-1$ and are called the *auxiliary components*. The widths of the auxiliary components are chosen to be $w_{n+1} = w_{n+2} = \cdots = w_{2n-1} = w_d$, and the thicknesses of these components are chosen to be $h_{n+1} = h_{n+2} = \cdots = h_{2n-1} = h_d$. The lengths of the auxiliary components are chosen to be $l_{n+1} = l_{n+2} = \cdots = l_{2n-1} = l_s \ll l_d$. Having the auxiliary components much shorter

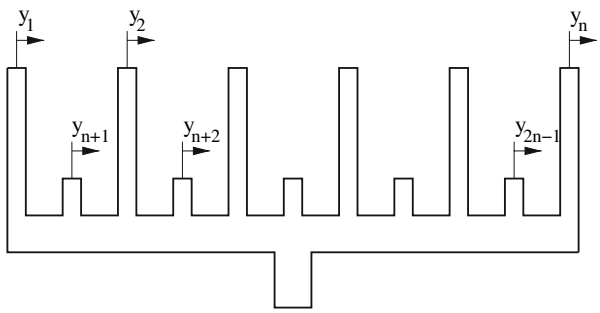

Fig. 5 A non-axisymmetric periodic structure with n principal components is augmented by adding $n-1$ small auxiliary components. The added components suppress vibration localization

than the principal components turns out to be crucially important in suppressing vibration localization in mistuned non-axisymmetric periodic structure; see also [1–3].

The generalized coordinates corresponding to the augmented structure satisfy

$$\tilde{M}\ddot{\tilde{\mathbf{q}}}(t)+\alpha\tilde{M}\dot{\tilde{\mathbf{q}}}(t)+\tilde{K}\tilde{\mathbf{q}}(t)=-\tilde{\mathbf{f}}u_a(t), \tag{23}$$

for all $t \geq 0$. In Eq. 23, the vector of generalized coordinates is

$$\tilde{\mathbf{q}}(t)=\begin{bmatrix}\mathbf{q}(t)\\ \mathbf{q}_a(t)\end{bmatrix}\in\mathbb{R}^{2n-1}, \tag{24}$$

for all $t \geq 0$, where $\mathbf{q}(t)$ is that in Eq. 9 and

$$\mathbf{q}_a(t)=[q_{n+1}(t)\quad q_{n+2}(t)\cdots q_{2n-1}(t)]^T\in\mathbb{R}^{n-1}, \tag{25}$$

is the vector of generalized coordinates corresponding to the auxiliary components. The initial conditions of system (23) are $\tilde{\mathbf{q}}(0)=\mathbf{0}_{2n-1}$ and $\dot{\tilde{\mathbf{q}}}(0)=\mathbf{0}_{2n-1}$. The input (influence) vector corresponding to system (23) is

$$\tilde{\mathbf{f}}=\begin{bmatrix}\mathbf{f}\\ \mathbf{f}_a\end{bmatrix}\in\mathbb{R}^{2n-1}, \tag{26}$$

where $\mathbf{f}$ is that in Eq. 10 and

$$\mathbf{f}_a=[f_{n+1}\quad f_{n+2}\cdots f_{2n-1}]^T\in\mathbb{R}^{n-1}, \tag{27}$$

is the input vector through which the acceleration $u_a(\cdot)$ is applied to the auxiliary components; the elements of $\mathbf{f}_a$ are computed via Eq. 5. The mass matrix of system (23) is

$$\tilde{M}=\begin{bmatrix}M & 0\\ 0 & M_a\end{bmatrix}\in\mathbb{R}^{2n-1\times 2n-1}, \tag{28}$$

where M is that in Eq. 11a and

$$M_a=\text{diag}[m_{n+1},m_{n+2},\ldots,m_{2n-1}]\in\mathbb{R}^{n-1\times n-1}, \tag{29}$$

where $m_{n+1},m_{n+2},\ldots,m_{2n-1}$ are computed via Eq. 5. The stiffness matrix of system (23) is

$$\tilde{K}=\begin{bmatrix}K_{11} & K_{12}\\ K_{12}^T & K_{22}\end{bmatrix}\in\mathbb{R}^{2n-1\times 2n-1}, \tag{30}$$

where

$$K_{11}=\text{diag}[k_1+\gamma k_c,k_2+2\gamma k_c,k_3+2\gamma k_c,\ldots,k_{n-1}+2\gamma k_c,k_n+\gamma k_c]\in\mathbb{R}^{n\times n}, \tag{31a}$$

$$K_{22}=\text{diag}[k_{n+1}+2\gamma k_c,k_{n+2}+2\gamma k_c,\ldots,k_{2n-1}+2\gamma k_c]\in\mathbb{R}^{n-1\times n-1}, \tag{31b}$$

$$K_{12}=\begin{bmatrix}-\gamma k_c & 0 & 0 & 0\cdots 0 & 0 & 0\\ -\gamma k_c & -\gamma k_c & 0 & 0\cdots 0 & 0 & 0\\ 0 & -\gamma k_c & -\gamma k_c & 0\cdots 0 & 0 & 0\\ \vdots & \vdots & \vdots & \vdots\ldots\vdots & \vdots & \vdots\\ 0 & 0 & 0 & 0\vdots 0 & -\gamma k_c & -\gamma k_c\\ 0 & 0 & 0 & 0\cdots 0 & 0 & -\gamma k_c\end{bmatrix}\in\mathbb{R}^{n\times n-1}, \tag{31c}$$

where $k_{n+1}, k_{n+2}, \ldots, k_{2n-1}$ are computed via Eq. 5, and $\gamma > 1$ represents increase in the coupling between the adjacent components of the augmented structure due to the proximity of such components.

For system (23), let $g_i(s)$ denote the transfer function from $u_a(\cdot)$ to $\tilde{q}_i(\cdot)$ for an $i = 1, 2, \ldots, 2n-1$. From Eq. 23, it follows that

$$\begin{bmatrix} g_1(s) \\ g_2(s) \\ \vdots \\ g_{2n-1}(s) \end{bmatrix} = -a_4(\tilde{M}s^2 + \alpha\tilde{M}s + \tilde{K})^{-1}\tilde{\mathbf{f}}. \tag{32}$$

The occurrence of vibration localization in the principal components due to mistunings in both principal and auxiliary components is easily determined when $\|g_1\|_\infty, \|g_2\|_\infty, \ldots, \|g_n\|_\infty$ are known. If these norms do not differ much from each other, then vibration localization does not occur. Note that vibration localization in the principal components is of primary interest. If vibration localization in the auxiliary components is to be studied, the H_∞-norms of the transfer functions corresponding to those components should be computed. As will be shown in the following example, the auxiliary components suppress vibration localization in the principal components, while do not let such phenomenon occur in themselves either.

Example 4.1 Consider the comb drive in Example 3.1. The (principal) components of the comb drive are numbered by $1, 2, \ldots, 6$. Five auxiliary components are added to the comb drive and numbered by $7, 8, \ldots, 11$. The desired length of the auxiliary components is chosen $l_s = 0.05 l_d = 5\,\mu\text{m}$. The desired widths and thicknesses of the auxiliary components are, respectively, w_d and h_d, given in Eq. 18.

To confirm the efficacy of the auxiliary components in desensitizing $\|g_1\|_\infty, \|g_2\|_\infty, \ldots, \|g_6\|_\infty$ to mistunings, and hence in suppressing vibration localization, let the dimensions of the auxiliary components be

$$\begin{array}{lll} l_7 = 5\,\mu\text{m}, & w_7 = 7.01\,\mu\text{m}, & h_7 = 2.05\,\mu\text{m}, \\ l_8 = 5.02\,\mu\text{m}, & w_8 = 7.05\,\mu\text{m}, & h_8 = 2.01\,\mu\text{m}, \\ l_9 = 4.98\,\mu\text{m}, & w_9 = 6.95\,\mu\text{m}, & h_9 = 1.99\,\mu\text{m}, \\ l_{10} = 4.99\,\mu\text{m}, & w_{10} = 6.99\,\mu\text{m}, & h_{10} = 2\,\mu\text{m}, \\ l_{11} = 5.01\,\mu\text{m}, & w_{11} = 7.02\,\mu\text{m}, & h_{11} = 2.02\,\mu\text{m}. \end{array} \tag{33}$$

The dimensions of the auxiliary components differ from the desired dimensions. Since the components of the augmented comb drive are closer to each other, it is inferred that the coupling between the adjacent components is stronger. Stronger coupling is taken into account by choosing $\gamma = 2$ in Eq. 31.

The H_∞-norms of $g_1(s), g_2(s), \ldots, g_{11}(s)$ are computed using MATLAB; they are

$$\begin{array}{lll} \|g_1\|_\infty = 0.6395 \times 10^{-10}\,\text{s}^2, & \|g_2\|_\infty = 0.5630 \times 10^{-10}\,\text{s}^2, & \|g_3\|_\infty = 0.6110 \times 10^{-10}\,\text{s}^2, \\ \|g_4\|_\infty = 0.5112 \times 10^{-10}\,\text{s}^2, & \|g_5\|_\infty = 0.5893 \times 10^{-10}\,\text{s}^2, & \|g_6\|_\infty = 0.5647 \times 10^{-10}\,\text{s}^2, \\ \|g_7\|_\infty = 0.1480 \times 10^{-12}\,\text{s}^2, & \|g_8\|_\infty = 0.1521 \times 10^{-12}\,\text{s}^2, & \|g_9\|_\infty = 0.1513 \times 10^{-12}\,\text{s}^2, \\ \|g_{10}\|_\infty = 0.1511 \times 10^{-12}\,\text{s}^2, & \|g_{11}\|_\infty = 0.1507 \times 10^{-12}\,\text{s}^2. & \end{array} \tag{34}$$

It is clear that the H_∞-norms of the transfer functions corresponding to the principal components are almost equal and closer to those in Eq. 20; so are almost equal those corresponding to the auxiliary components. That is, even though there are mistunings in all components of the augmented comb drive, the principal components have almost the same dynamics. This implies that vibration localization is suppressed. To witness, the Bode magnitude plots of $g_1(s), g_2(s), \ldots, g_{11}(s)$ are depicted in Fig. 6a. The Bode magnitude plots of $g_1(s), g_2(s), \ldots, g_6(s)$ are magnified and shown in Fig. 6b. It is also evident from these plots that the effect of coupling is reduced and the comb drive components do not have several resonant frequencies, unlike the case shown in Fig. 4.

5 Mathematical justification

Suppression of vibration localization in mistuned non-axisymmetric periodic structures by the auxiliary components was illustrated in Example 4.1. In this section, it is rigorously proved that the auxiliary components indeed suppress

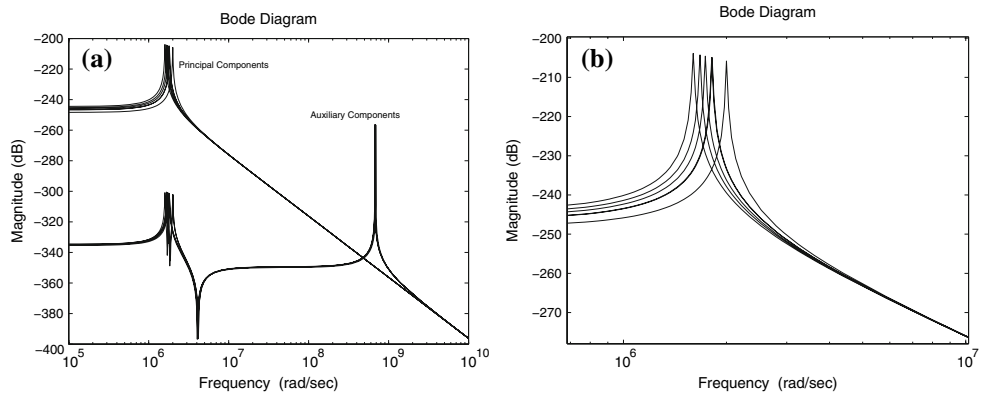

Fig. 6 **(a)** The Bode magnitude plots of transfer functions corresponding to the principal and auxiliary components of the augmented comb drive in Example 4.1; **(b)** The magnification of the Bode magnitude plots corresponding to transfer functions of the principal components

vibration localization. In other words, it will be shown that the small auxiliary components added to a mistuned structure make the H_∞-norms of the transfer functions corresponding to the principal components almost equal and insensitive to mistunings in all components. The analysis in this section follows those in [1,3]. Details of the analysis, however, are different, since the mathematical models of the structure components differ from those in [1,3].

System (23) can be written as

$$\begin{bmatrix} M & 0 \\ 0 & M_a \end{bmatrix} \begin{bmatrix} \ddot{\mathbf{q}}(t) \\ \ddot{\mathbf{q}}_a(t) \end{bmatrix} + \alpha \begin{bmatrix} M & 0 \\ 0 & M_a \end{bmatrix} \begin{bmatrix} \dot{\mathbf{q}}(t) \\ \dot{\mathbf{q}}_a(t) \end{bmatrix} + \begin{bmatrix} K_{11} & K_{12} \\ K_{12}^T & K_{22} \end{bmatrix} \begin{bmatrix} \mathbf{q}(t) \\ \mathbf{q}_a(t) \end{bmatrix} = - \begin{bmatrix} \mathbf{f} \\ \mathbf{f}_a \end{bmatrix} u_a(t), \tag{35}$$

for all $t \geq 0$, where $\mathbf{q}(0) = \mathbf{0}_n$, $\mathbf{q}_a(0) = \mathbf{0}_{n-1}$, $\dot{\mathbf{q}}(0) = \mathbf{0}_n$, and $\dot{\mathbf{q}}_a(0) = \mathbf{0}_{n-1}$.

Vibration localization in system (35) is studied in the following. The conclusion to be reached is that, if $0 < l_s \ll l_d$, then vibration localization in system (35) does not occur.

It is clear that the lengths of the auxiliary components satisfy the following relation:

$$l_{n+i} = \varepsilon \bar{l}_{n+i}, \tag{36}$$

for all $i = 1, 2, \ldots, n-1$, where

$$\varepsilon := \frac{l_s}{l_d}, \tag{37a}$$

$$\bar{l}_{n+i} = \frac{l_d l_{n+i}}{l_s}. \tag{37b}$$

From Eq. 37, it follows that

$$M_a = \varepsilon \bar{M}_a, \quad K_{22} = \frac{\bar{K}_{22}}{\varepsilon^3}, \quad \mathbf{f}_a = \varepsilon \bar{\mathbf{f}}_a, \tag{38}$$

where

$$\bar{M}_a = a_1 \rho \ \text{diag}[w_{n+1} h_{n+1} \bar{l}_{n+1}, w_{n+2} h_{n+2} \bar{l}_{n+2}, \ldots, w_{2n-1} h_{2n-1} \bar{l}_{2n-1}] \in \mathbb{R}^{n-1 \times n-1}, \tag{39}$$

$$\bar{K}_{22} = \text{diag} \left[\frac{a_2 E w_{n+1} h_{n+1}^3}{3 \bar{l}_{n+1}^3} + 2\varepsilon^3 \gamma k_c, \frac{a_2 E w_{n+2} h_{n+2}^3}{3 \bar{l}_{n+2}^3} + 2\varepsilon^3 \gamma k_c, \ldots, \frac{a_2 E w_{2n-1} h_{2n-1}^3}{3 \bar{l}_{2n-1}^3} + 2\varepsilon^3 \gamma k_c \right] \in \mathbb{R}^{n-1 \times n-1}, \tag{40}$$

$$\bar{\mathbf{f}}_a = a_3\rho[w_{n+1}h_{n+1}\bar{l}_{n+1}, w_{n+2}h_{n+2}\bar{l}_{n+2}, \ldots, w_{2n-1}h_{2n-1}\bar{l}_{2n-1}] \in \mathbb{R}^{n-1}. \tag{41}$$

Using Eq. 38, system (35) can be written as

$$M\ddot{\mathbf{q}}(t) + \alpha M\dot{\mathbf{q}}(t) + K_{11}\mathbf{q}(t) + K_{12}\mathbf{q}_a(t) = -\mathbf{f}\, u_a(t), \tag{42a}$$

$$\varepsilon^4\bar{M}_a\ddot{\mathbf{q}}_a(t) + \varepsilon^4\alpha\bar{M}_a\dot{\mathbf{q}}_a(t) + \varepsilon^3K_{12}^T\mathbf{q}(t) + \bar{K}_{22}\mathbf{q}_a(t) = -\varepsilon^4\bar{\mathbf{f}}_a u_a(t), \tag{42b}$$

for all $t \geq 0$, where $\mathbf{q}(0) = \mathbf{0}_n$, $\mathbf{q}_a(0) = \mathbf{0}_{n-1}$, $\dot{\mathbf{q}}(0) = \mathbf{0}_n$, and $\dot{\mathbf{q}}_a(0) = \mathbf{0}_{n-1}$.

It is noted that $0 < \varepsilon \ll 1$ since $l_s \ll l_d$. Small ε implies that there is dichotomy in the dynamics of system (42): the vector $\mathbf{q}(\cdot)$ evolves slowly in time, whereas the vector $\mathbf{q}_a(\cdot)$ evolves fast. Due to this dichotomy, system (42) can be studied by the singular perturbation method see, e.g., [32–35] and references therein. According to this method, for sufficiently small ε, the dynamics of system (42) can be approximated by the dynamics of two subsystems. These subsystems are the slow and fast subsystems and are presented in the following.

5.1 Slow subsystem

The slow subsystem is an n-dimensional system obtained as follows. In Eq. 42b, first set $\varepsilon = 0$, and then solve for $\mathbf{q}_a(\cdot)$. The result is

$$\mathbf{q}_a(t) = \mathbf{0}_{n-1}, \tag{43}$$

for all $t \geq 0$. Substituting $\mathbf{q}_a(\cdot)$ in Eq. 42a, the representation of the slow subsystem is obtained as

$$M\ddot{\mathbf{q}}(t) + \alpha M\dot{\mathbf{q}}(t) + K_{11}\mathbf{q}(t) = -\mathbf{f}\, u_a(t), \tag{44}$$

for all $t \geq 0$, where $\mathbf{q}(0) = \mathbf{0}_n$ and $\dot{\mathbf{q}}(0) = \mathbf{0}_n$.

Since M and K_{11} are diagonal matrices, system (44) is a set of n decoupled second-order systems given by

$$m_i\ddot{q}_i(t) + \alpha m_i\dot{q}_i(t) + (k_i + \gamma k_c)q_i(t) = -f_i u_a(t), \quad \text{for } i = 1, n, \tag{45a}$$

$$m_i\ddot{q}_i(t) + \alpha m_i\dot{q}_i(t) + (k_i + 2\gamma k_c)q_i(t) = -f_i u_a(t), \quad \text{for all } i = 2, \ldots, n-1, \tag{45b}$$

for all $t \geq 0$, where $q_i(t) \in \mathbb{R}$, and $q_i(0) = 0$ and $\dot{q}_i(0) = 0$ for all $i = 1, \ldots, n$.

Having the simple representation in Eq. 45, the transfer function from $u_a(\cdot)$ to $y_i(l_i, \cdot) = \phi(l_i)q_i(\cdot)$ is readily obtained as

$$g_i(s) = -\frac{a_4 f_i}{m_i s^2 + \alpha m_i s + k_i + \gamma k_c}, \quad \text{for } i = 1, n, \tag{46a}$$

$$g_i(s) = -\frac{a_4 f_i}{m_i s^2 + \alpha m_i s + k_i + 2\gamma k_c}, \quad \text{for all } i = 2, \ldots, n-1, \tag{46b}$$

where a_4 is given in Eq. 14.

It can be easily verified that the resonant frequencies of the systems represented by the transfer functions in Eqs. 46a and 46b are, respectively,

$$\omega_i{}^* = \left(\frac{a_2 E w_i {h_i}^3/(3{l_i}^3) + \gamma k_c}{a_1\rho w_i h_i l_i} - \frac{\alpha^2}{2}\right)^{1/2}, \quad \text{for } i = 1, n, \tag{47a}$$

$$\omega_i{}^* = \left(\frac{a_2 E w_i {h_i}^3/(3{l_i}^3) + 2\gamma k_c}{a_1\rho w_i h_i l_i} - \frac{\alpha^2}{2}\right)^{1/2}, \quad \text{for all } i = 2, \ldots, n-1. \tag{47b}$$

The H_∞-norms of the transfer functions in Eqs. 46a and 46b are, respectively,

$$\|g_i\|_\infty = \frac{a_3 a_4}{\alpha a_1\left(\frac{a_2 E w_i {h_i}^3/(3{l_i}^3)+\gamma k_c}{a_1\rho w_i h_i l_i} - \frac{\alpha^2}{4}\right)^{1/2}}, \quad \text{for } i = 1, n, \tag{48a}$$

$$\|g_i\|_\infty = \frac{a_3 a_4}{\alpha a_1 \left(\frac{a_2 E w_i {h_i}^3/(3{l_i}^3)+2\gamma k_c}{a_1 \rho w_i h_i l_i} - \frac{\alpha^2}{4} \right)^{1/2}}, \quad \text{for all } i = 2, \ldots, n-1. \tag{48b}$$

Since k_c is small and l_i, w_i, and h_i are close to l_d, w_d and h_d, respectively, for all $i = 1, 2, \ldots, n$, it follows that ${\omega_1}^*, {\omega_2}^*, \ldots, {\omega_n}^*$ in Eq. 47 are close to each other, so are $\|g_1\|_\infty, \|g_2\|_\infty, \ldots, \|g_n\|_\infty$ in Eq. 48.

5.2 Fast subsystem

The fast subsystem is an $(n-1)$-dimensional system obtained as follows. In system (42), set $t = \varepsilon^2 \tau$. The result is

$$M \frac{\mathrm{d}^2 \mathbf{q}(\tau)}{\mathrm{d}\tau^2} + \varepsilon^2 \alpha M \frac{\mathrm{d}\mathbf{q}(\tau)}{\mathrm{d}\tau} + \varepsilon^4 [K_{11} \mathbf{q}(\tau) + K_{12} \mathbf{q}_a(\tau)] = -\varepsilon^4 \mathbf{f} u_a(\tau), \tag{49a}$$

$$\bar{M}_a \frac{\mathrm{d}^2 \mathbf{q}_a(\tau)}{\mathrm{d}\tau^2} + \varepsilon^2 \alpha \bar{M}_a \frac{\mathrm{d}\mathbf{q}_a(\tau)}{\mathrm{d}\tau} + \varepsilon^3 {K_{12}}^T \mathbf{q}(\tau) + \bar{K}_{22} \mathbf{q}_a(\tau) = -\varepsilon^4 \bar{\mathbf{f}}_a u_a(\tau), \tag{49b}$$

for all $\tau \geq 0$, where $\mathbf{q}(0) = \mathbf{0}_n$, $\mathbf{q}_a(0) = \mathbf{0}_{n-1}$, $\mathrm{d}\mathbf{q}(\tau)/\mathrm{d}(\tau) = \mathbf{0}_n$, and $\mathrm{d}\mathbf{q}_a(\tau)/\mathrm{d}\tau = \mathbf{0}_{n-1}$ at $\tau = 0$. Setting $\varepsilon = 0$ in Eq. 49a yields that $\mathbf{q}(\tau) = \mathbf{0}_n$ for all $\tau \geq 0$, and hence Eq. 49b can be written as

$$\bar{M}_a \frac{\mathrm{d}^2 \mathbf{q}_a(\tau)}{\mathrm{d}\tau^2} + \varepsilon^2 \alpha \bar{M}_a \frac{\mathrm{d}\mathbf{q}_a(\tau)}{\mathrm{d}\tau} + \bar{K}_{22} \mathbf{q}_a(\tau) = -\varepsilon^4 \bar{\mathbf{f}}_a u_a(\tau), \tag{50}$$

for all $\tau \geq 0$, where $\mathbf{q}_a(0) = \mathbf{0}_{n-1}$ and $\mathrm{d}\mathbf{q}_a(\tau)/\mathrm{d}\tau = \mathbf{0}_{n-1}$ at $\tau = 0$. System (50) is the representation of the fast subsystem. Since $\bar{M}_a$ and $\bar{K}_{22}$ are diagonal matrices, system (50) is a set of $n-1$ decoupled second-order systems, one of which for an $i = 1, 2, \ldots, n-1$ is

$$a_1 \rho w_{n+i} h_{n+i} \bar{l}_{n+i} \frac{\mathrm{d}^2 q_{n+i}(\tau)}{\mathrm{d}\tau^2} + \varepsilon^2 \alpha a_1 \rho w_{n+i} h_{n+i} \bar{l}_{n+i} \frac{\mathrm{d}q_{n+i}(\tau)}{\mathrm{d}\tau} + \left[\frac{a_2 E w_{n+i} h_{n+i}^3}{3\bar{l}_{n+i}^3} + 2\varepsilon^3 \gamma k_c \right] q_{n+i}(\tau) = -\varepsilon^4 a_3 \rho w_{n+i} h_{n+i} \bar{l}_{n+i} u_a(\tau), \tag{51}$$

for all $\tau \geq 0$, where $q_{n+i}(\tau) \in \mathbb{R}$, and $q_{n+i}(0) = 0$ and $\mathrm{d}q_{n+i}(\tau)/\mathrm{d}\tau = 0$ at $\tau = 0$. Setting $\tau = t/\varepsilon^2$ and using Eq. 36, one can write Eq. 51 as

$$m_{n+i} \ddot{q}_{n+i}(t) + \alpha m_{n+i} \dot{q}_{n+i}(t) + (k_{n+i} + 2\gamma k_c) q_{n+i}(t) = -f_{n+i} u_a(t), \tag{52}$$

for all $t \geq 0$ and $i = 1, \ldots, n-1$, where m_{n+i}, k_{n+i}, and f_{n+i} are computed via Eq. 5, and $q_{n+i}(0) = 0$ and $\dot{q}_{n+i}(0) = 0$.

Having the simple representation in Eq. 52, the transfer function from $u_a(\cdot)$ to $\mathrm{y}_{n+i}(\cdot) = \phi(l_{n+i}) q_{n+i}(\cdot)$ is obtained as

$$g_{n+i}(s) = -\frac{a_4 f_{n+i}}{m_{n+i} s^2 + \alpha m_{n+i} s + k_{n+i} + 2\gamma k_c}, \tag{53}$$

for all $i = 1, 2, \ldots, n-1$.

The resonant frequency of the system represented by the transfer function in Eq. 53 is

$${\omega}_{n+i}^* = \left(\frac{a_2 E w_{n+i} h_{n+i}^3/(3l_{n+i}^3) + 2\gamma k_c}{a_1 \rho w_{n+i} h_{n+i} l_{n+i}} - \frac{\alpha^2}{2} \right)^{1/2}, \tag{54}$$

for all $i = 1, 2, \ldots, n-1$. The H_∞-norm of the transfer function in Eq. 53 is

$$\|g_{n+i}\|_\infty = \frac{a_3 a_4}{\alpha a_1 \left(\frac{a_2 E w_{n+i} h_{n+i}^3/(3l_{n+i}^3)+2\gamma k_c}{a_1 \rho w_{n+i} h_{n+i} l_{n+i}} - \frac{\alpha^2}{4} \right)^{1/2}}, \tag{55}$$

for all $i = 1, 2, \ldots, n-1$. Since k_c is small and l_{n+i}, w_{n+i}, and h_{n+i} are close to l_s, w_d, and h_d, respectively, for all $i = 1, 2, \ldots, n-1$, it follows that ${\omega}_{n+1}^*, {\omega}_{n+2}^*, \ldots, {\omega}_{2n-1}^*$ in Eq. 54 are close to each other, so are $\|g_{n+1}\|_\infty, \|g_{n+2}\|_\infty, \ldots, \|g_{2n-1}\|_\infty$ in Eq. 55.

Remarks Several conclusions regarding the slow and fast subsystems are now drawn:

(1) Since $l_s \ll l_d$ the H_∞-norms in Eqs. 48 and 55 satisfy the following inequality:

$$\|g_{n+j}\|_\infty \ll \|g_i\|_\infty, \tag{56}$$

for any $i = 1, 2, \ldots, n$ and $j = 1, 2, \ldots, n-1$.

(2) For lightly damped structures, it follows from Eqs. 48 and 55 that

$$\|g_i\|_\infty = \frac{a_3 a_4}{\alpha (a_1 a_2)^{1/2}} \left(\frac{3\rho}{E}\right)^{1/2} \frac{{l_i}^2}{h_i}, \quad \|g_{n+j}\|_\infty = \frac{a_3 a_4}{\alpha (a_1 a_2)^{1/2}} \left(\frac{3\rho}{E}\right)^{1/2} \frac{l_{n+j}^2}{h_{n+j}}, \tag{57a}$$

$$\frac{\|g_{n+j}\|_\infty}{\|g_i\|_\infty} \approx \varepsilon^2, \tag{57b}$$

for any $i = 1, 2, \ldots, n$ and $j = 1, 2, \ldots, n-1$. For $\varepsilon = 0.05$, the ratio in Eq. 57b justifies the H_∞-norms of the transfer functions corresponding to the principal and auxiliary components of the comb drive in Example 4.1 given in Eq. 34; see also Fig. 6.

(3) For lightly damped structures, it is concluded from Eqs. 47 and 54 that the resonant frequencies of the slow and fast subsystems satisfy the following relation:

$$\frac{\omega_{n+j}^*}{\omega_i^*} \approx \frac{{l_i}^2}{l_{n+j}^2} \approx \frac{1}{\varepsilon^2} \gg 1, \tag{58}$$

for any $i = 1, 2, \ldots, n$ and $j = 1, 2, \ldots, n-1$. For $\varepsilon = 0.05$, the ratio in Eq. 58 justifies the resonant frequencies of the principal and auxiliary components of the comb drive in Example 4.1; see Fig. 6.

Having the slow and fast subsystems given by Eqs. 45 and 52, respectively, one may draw conclusions regarding the augmented structure using the singular perturbation method. According to this method, for sufficiently small ε, the dynamics of the $(2n-1)$-dimensional augmented structure in Eq. 23 (equivalently Eq. 35) can be approximated by those of the n-dimensional slow subsystem and the $(n-1)$-dimensional fast subsystem over large and small time scales, respectively, Therefore, the transfer functions corresponding to the principal (respectively, auxiliary) components can be approximated at low (high) frequencies by those corresponding to the slow (fast) subsystem given by Eq. 46 (Eq. 53). From Eq. 48, or Eq. 57a for lightly damped structures, it is evident that the H_∞-norms of the transfer functions corresponding to the slow subsystems are almost equal; hence, so are those of the transfer functions corresponding to the principal components. That is, the H_∞-norms of the transfer functions of the principal components are insensitive to mistunings. In other words, vibration localization does not occur in the principal components. It is also concluded that: (i) the H_∞-norms of the transfer functions corresponding to the auxiliary components are almost equal to those in Eq. 55, or those in Eq. 57a for lightly damped structures; (ii) by inequality (56), or Eq. 57b for lightly damped structures, these norms are much smaller than those of the transfer functions corresponding to the principal components; (iii) by inequality (58), for lightly damped structures, the resonant frequencies of the auxiliary components are much higher than those of the principal components. Thus, (i) vibration localization does not occur in the auxiliary components; (ii) the amplitudes of vibration of such components are small.

6 Conclusions

In this paper, mistuned non-axisymmetric periodic structures have been studied. Mistunings are due to slight differences in the geometry and material properties of components of such structures. Small mistunings can cause significant differences in the dynamics of components of structures. It is well known that in mistuned periodic structures, some components may vibrate with small amplitudes, while some others may vibrate with significantly larger amplitudes. Such a behavior is known as vibration localization and is undesirable.

In this paper, it was shown that vibration localization in mistuned non-axisymmetric periodic structures can be suppressed by the passive technique proposed in [1–3]. The suppression is achieved by adding small components between components of structures. The occurrence of vibration localization in fingers of a comb drive and suppression of such phenomenon by adding small components between the fingers were shown via examples.

Following the steps taken in this paper, two conclusions can be drawn. In the following, these conclusions are stated without details.

(i) A non-axisymmetric structure can be augmented by adding $n + 1$ small auxiliary components, where two of such components are added to both ends of the structure. This arrangement guarantees that the principal components at both ends of the structure are surrounded by two auxiliary components. The augmented structure is slightly different from what is presented in the paper. However, vibration localization is suppressed in the augmented structure.

(ii) Adding small auxiliary components between the principal components of structures, periodic or otherwise, has a very important consequence. Consider a structure which is not periodic, that is, its components are not designed and fabricated to be identical. For instance, consider the structure in Fig. 1, where its components have various sizes. There is certainly coupling between the structure components. Suppose that small components, which are smaller than the smallest component of the structure, are added between the structure components. The added small components decouple the structure components. The decoupling effect of the small components can be established by applying the mathematical technique used in this paper.

By (ii), suppression of vibration localization in periodic structures can be explained by a different argument. When small components are added to a periodic structure, the structure components are decoupled. Components of a periodic structure have same dynamics when they are decoupled. This implies that vibration localization does not occur.

References

1. Shahruz SM (2004) Technique to eliminate vibration localization. Rev Sci Instruments 75(11):4629–4635
2. Shahruz SM (2005) Elimination of vibration localization in mistuned periodic structures. J Sound Vibrat 281(1–2):452–462
3. Shahruz SM (2005) Elimination of vibration localization: a mathematical justification. J Sound Vibrat 283(1–2):449–458
4. Anderson PW (1958) Absence of diffusion in certain random lattices. Phys Rev 109(5):1492–1505
5. Orgun CO (1991) Vibration localization in multiple disk stacks. Master of Science Thesis, Department of Mechanical Engineering, University of California, Berkeley
6. Castanier MP, Pierre C (1997) Consideration on the benefits of intensional blade mistuning for the forced response of turbomachinery rotors. In: Simitses GJ (ed) Analysis and design issues for modern aerospace vehicles. The American Society of Mechanical Engineers, New York, NY, pp 419–425
7. Bendiksen OO (2000) Localization phenomena in structural dynamics. Chaos, Solitons Fractals 11(10):1621–1660
8. Tang J, Wang KW (2003) Vibration delocalization of nearly periodic structures using coupled piezoelectric networks. J Vibration Acoustics 125(1):95–108
9. Yoo HH, Kim JY, Inman DJ (2003) Vibration localization of simplified mistuned cyclic structures undertaking external harmonic force. J Sound Vibration 261(5):859–870
10. Huang B-W (2006) Effect of number of blades and distribution of cracks on vibration localization in a cracked pre-twisted blade system. Int J Mech Sci 48(1):1–10
11. Fang X, Tang J, Jordan E, Murphy KD (2006) Crack induced vibration localization in simplified bladed-disk structures. J Sound Vibration 291(1–2):395–418
12. Judge JA, Houston BH, Photiadis DM, Herdic PC (2006) Effects of disorder in one and two-dimensional micromechanical resonator arrays for filtering. J Sound Vibration 290(3–5):1119–1140
13. Shin SH, Lee SJ, Yoo HH (2006) Statistical characteristics of frequency response localization in nearly periodic systems. J Sound Vibrat 290(4–5):1039–1050
14. Legtenberg R, Groeneveld AW, Elwenspoek M (1996) Comb-drive actuators for large displacements. J Micromech Microeng 6(3):320–329
15. Ye W, Mukherjee S, MacDonald NC (1998) Optimal shape design of an electrostatic comb drive in microelectromechanical systems. J Microelectromech Syst 7(1):16–26
16. Stark B (ed) (1999) MEMS Reliability assurance guidances for space applications. Jet Propulsion Laboratory, Pasadena, CA, JPL Publication 99-1

17. Elwenspoek M, Wiergerink R (2001) Mechanical microsensors. Springer-Verlag, New York, NY
18. Gardner JW, Varadan VK, Awadelkarim OO (2001) Microsensors, MEMS, and smart devices. Wiley, Chichester, UK
19. Ananthasuresh GK (ed) (2003) Optimal synthesis methods for MEMS. Kluwer Academic Publishers, Norwell, MA
20. Chen C, Lee C, Lai Y-J, Chen W (2003) Development and application of lateral comb drive actuator. Japanese J Appl Phys 42(Part 1, No. 6B):4059–4062
21. Grade JD, Jerman H, Kenny TW (2003) Design of large deflection electrostatic actuators. J Microelectromech Syst 12(3):335–343
22. Jensen BD, Mutlu S, Miller S, Kurabayashi K, Allen JJ (2003) Shaped comb fingers for tailored electromechanical restoring force. J Microelectromech Syst 12(3):373–383
23. Zhou G, Dowd P (2003) Tilted folded-beam suspension for extending the stable travel range of comb-drive actuators. J Micromech Microeng 13(2):178–183
24. Beeby S, Ensell G, Kraft M, White N (2004) MEMS mechanical sensors. Artech House, Norwood, MA
25. De Los Santos HJ (2004) Introduction to microelectromechanical microwave systems, 2nd edn. Artech House, Norwood, MA
26. Johnstone RW, Parameswaran M (2004) An Introduction to surface-micromachining. Kluwer Academic Publishers, Norwell, MA
27. Maluf N, Williams K (2004) An introduction to microelectromechanical systems engineering, 2nd edn. Artech House, Norwood, MA
28. Shahruz SM (2006) Design of mechanical band-pass filters for energy scavenging. J Sound Vibrat 292(3–5):987–998
29. Shahruz SM (2006) Limits of performance of mechanical band-pass filters used in energy scavenging. J Sound Vibrat 293(1–2):449–461
30. Shahruz SM (2006) Design of mechanical band-pass filters with large frequency bands for energy scavenging. Mechatronics 16(9):523–531
31. MATLAB (1997) Mathworks, Inc., Natick, MA
32. Kokotovic PV, Khalil HK, O'Reilly J (1986) Singular perturbation methods in control: analysis and design. Academic Press, London, UK
33. O'Malley RE Jr (1991) Singular perturbation methods for ordinary differential equations. Springer-Verlag, New York, NY
34. Mishchenko EF, Kolesov YS, Kolesov AY, Rozov NK (1994) Asymptotic methods in singularly perturbed systems. Consultants Bureau, New York, NY
35. Naidu DS (2002) Singular perturbations and time scales in control theory and applications: an overview. Dyn Continuous, Discrete Impulsive Syst Ser B: Appl Algorithms 9(2):233–278